Appl. Phys. B 85, 25–31 (2006)
DOI: 10.1007/s00340-006-2368-x

Applied Physics B
Lasers and Optics

C.M. FAJARDO✉
J.D. SMITH
V. SICK

Sustained simultaneous high-speed imaging of scalar and velocity fields using a single laser

Department of Mechanical Engineering, The University of Michigan,
2026 W.E. Lay Automotive Laboratory, 1231 Beal Ave., Ann Arbor, MI 48109-2133, USA

Received: 18 April 2006/Revised version: 1 June 2006
Published online: 18 July 2006 •

ABSTRACT A high-speed technique that combines planar laser induced fluorescence (PLIF) detection of biacetyl and particle image velocimetry (PIV) for simultaneous imaging of scalar and velocity fields is demonstrated at a frame rate of 12 kHz for up to 32 500 consecutive frames. A single diode-pumped, frequency-tripled Nd-YAG laser was used for excitation. Wavelength-separated recording was achieved for Mie scattering from silicone oil droplets with a CMOS camera and for the red-shifted fluorescence from biacetyl with an image-intensified CMOS camera. Interference between PIV and PLIF tracers was found to be negligible. Cross-talk between PIV and PLIF signals was low and a strategy to completely eliminate it was devised and is discussed. The signal-to-noise ratio is about 9 for single-shot scalar images. Example image sequences were recorded in an atmospheric pressure air jet at Re = 2000.

PACS 42.62.Fi; 33.50.Dq; 06.30.Gv; 06.60.Jn

1 Introduction

The transport and mixing of passive scalars is relevant in a wide range of fields such as pollutant control, weather prediction, and combustion. In gasoline spark-ignition direct-injection (SIDI) engines, the equivalence ratio (i.e. the passive scalar) provides a quantitative measure of the fuel–air distribution inside the combustion chamber. For part-load applications, the equivalence ratio distribution in SIDI engines at the time of ignition is inhomogeneous. Fuel-rich areas near the spark plug are desirable to promote the onset and propagation of the early flame. However, a lean global equivalence ratio is maintained, which, among other benefits, improves fuel economy and thermal efficiency over conventional (port-fuel-injected) gasoline engines [1]. Inside the combustion chamber, fuel–air mixing, transport, and thus the equivalence ratio distribution are influenced by the flow field. The mean flow and turbulence also influence the development and propagation speed of the flame [2]. This suggests that a complete characterization of the physical processes surrounding the ignition event requires simultaneous velocity–scalar measurements under practical engine operating conditions. Furthermore, it is desirable to record images at rates that resolve the short time scales of turbulent flow processes (< ms) and cyclic variations.

Quantitative two-dimensional equivalence ratio distribution measurements using planar laser induced fluorescence (PLIF) in engines have been demonstrated with a variety of approaches [3]. Such measurements have become a valuable research and development tool. Two-dimensional flow data has also been obtained in engines using particle image velocimetry (PIV) either film based or with digital recording [4, 5]. Major shortcomings for both types of measurement usually are limited framing rate, with the exception of some studies that use a laser cluster and obtain eight consecutive frames at adequate rate [6], and lack of simultaneous measurement capability for equivalence ratio and flow fields. Recently, it was demonstrated that gas-phase equivalence ratio distributions can be measured in engines at sustained frame rates of 12 kHz [7]. Separately, it was also shown that velocity fields can be measured with PIV in engines at frame rates of 16 kHz [8]. These experiments, conducted under similar engine operating conditions, have provided data spanning the time period of injection, ignition, and early flame propagation.

The objective to simultaneously measure scalar quantities and flow fields has been pursued in previous studies. Amongst those are measurements of velocity fields and reaction intermediates like CH and/or OH radicals [9–11] in open, atmospheric pressure flames or in water jets [12]. The image rate for those studies was generally on the order of a few Hz with the exception of Hult et al. [10], where sequences of eight OH images were acquired at 13 kHz within the sequence while repeating the sequence acquisition at a few Hz. A single PIV frame was obtained within the time of each of these sequences. Characteristic to these studies is also the use of two separate laser systems for PLIF and PIV. Frank et al. [13] described two approaches for simultaneous concentration and velocity measurements using PLIF of biacetyl and PIV. A single-laser approach with excitation at 355 nm, as is used in the present study, is compared to a scheme where two laser systems are employed for increased signal strength. Repetition rates were reported in the few-Hz range. The next step in the development of simultaneous concentration and velocity measurement capabil-

✉ Fax: +1-734-764-4256, E-mail: cfajardo@engin.umich.edu

ity thus has to be efforts that address the limited frame rate and the number of frames that can be recorded.

The work presented here describes a new technique that combines high-speed PLIF and PIV in a single-laser, dual-camera setup to obtain two-dimensional, simultaneous velocity–scalar data. The feasibility study also includes an assessment of the following three objectives. First, an evaluation of whether the physical processes (e.g. adsorption, diffusion) that would cause biacetyl (seed for PLIF) and oil droplets (seed for PIV) to interact are negligible. This will be determined by evaluating the strength and degree of spatial intermittency of the PLIF signal intensity for the seeding density required in PIV; second, a determination of the level of signal cross-talk (if any) between PLIF and PIV images; third, an evaluation of whether the signal-to-noise ratio (SNR) is sufficient to obtain reliable velocity and scalar information in measurements in optical engines or similar devices.

Many challenges must be overcome to obtain reliable optical diagnostic data in internal combustion (IC) engines. These include unwanted scatter from engine walls and optical component alignment requirements. Since these issues have been successfully addressed in previous experiments [7, 8], this work has removed unnecessary complexity by demonstrating the technique in a cold jet flow. The selection of a relatively simple and well-characterized flow allows one to isolate the effect of tracer interaction in the absence of extraneous variables. This technique can eventually be applied in optical engines, gas turbines, and in other environments that require more complex experimental setups, to obtain simultaneous velocity–scalar data.

2 Experimental

The experimental setup, shown in Fig. 1, includes a single, frequency-tripled diode-pumped Nd:YAG laser (Quantronix Hawk) operated at 12 kHz and two high-speed CMOS cameras (Vision Research Phantom 7.1). At 12 kHz, the laser provides consecutive pulses of 100-ns duration and approximately 0.5 mJ of energy. The laser pulse frequency was not arbitrarily chosen. Considering that this technique will be extended to IC engine studies, 12 kHz was selected to obtain crank-angle resolution at 2000 RPM engine speed. Keeping in mind that the laser energy varies with pulse frequency, by selecting 12 kHz one can assess whether the intensity levels of the scattered and fluorescence signals are enough at this temporal resolution.

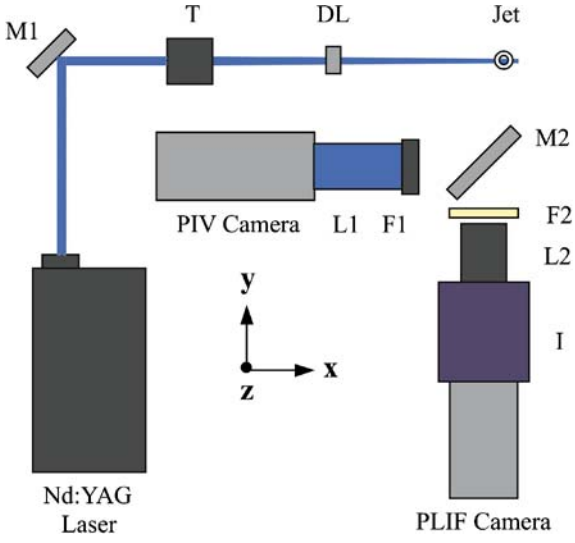

FIGURE 1 Setup for the velocity–scalar measurements in a jet using 355-nm excitation light. Legend: M1 – HR 355, HT 532 mirror, M2 – HR 355 mirror, T – focusing optics, DL – diverging lens, L1 – 105 mm UV lens, L2 – 105 mm Nikon Micro-Nikkor lens, F1 – 355-nm interference filter, F2 – GG 420 filter, I – image intensifier

The narrow, circular (~ 0.7 mm) 355-nm light beam was reflected using a HR 355/HT 532 45° turning mirror. Using light-sheet forming optics (Rodenstock Modular Focus), the beam was focused and expanded into a 1-mm-thick light sheet that illuminated the center line of the jet.

Though PLIF and PIV rely on fundamentally different physical processes, both techniques require the addition of tracers to the flow. Of course it is noted that naturally present species can be detected in many flow situations with PLIF (e.g. OH, NO, etc.). Here, however, fuel imaging is described with the common arrangement of using a non-fluorescing fuel and a fluorescence tracer. For PIV, air was mixed with silicon oil (Dow Corning 510R) droplets produced by a six-jet atomizer (TSI model 9306). Biacetyl was introduced through a bubbling apparatus that allowed line air to pass through liquid biacetyl. A bypass valve was also installed to either increase or decrease the fraction of the air bubbled through the biacetyl, which, in turn, either increased or decreased the registered biacetyl signal. The oil–air and biacetyl–air mixtures merged into a single line and mixed over a length of 20 cm before reaching a circular, 7 mm inner diameter stainless steel pipe. Rough edges at the pipe exit promoted instabilities in the jet. This was desirable in the context of the present work to enhance vortex shedding. The oil–air and biacetyl–air flow rates were adjusted to provide enough signal for the PLIF measurement and the required seeding density for the PIV measurements. Estimated biacetyl mole fractions in the core portion of the jet are on the order of 0.04. This value is based on the vapor pressure of biacetyl, assuming saturation of the air with biacetyl in the bubbler and an even split of the flow rates from the biacetyl and the PIV seeding systems. Oil droplet seeding homogeneity and density were checked by isolating 32×32 pixel windows from the raw images using an in situ visualization utility. An average of 10–15 particle images is desirable for best PIV results. It was also important to ensure that the exit flow speed could be resolved with the 83.3 μs (i.e. 1/12 kHz) laser pulse delay. This was accomplished by adjusting the flow rate until the maximum particle shift between laser pulses did not exceed 1/4 of the interrogation window size [14–16].

A 101 mm HR 355/45 deg. mirror was located in front of the CMOS cameras. The elastically scattered light from the 1-μm-diameter oil droplets used for the PIV measurements was reflected via this mirror and focused by a 105 mm f/4.5 UV lens (Coastal Optics SLR) onto the first (PIV) camera. A 355-nm interference filter was placed in front of the PIV camera to minimize the level of background signal recorded. Biacetyl fluorescence was collected with

a 105 mm f/1.4 lens (Nikon Micro-Nikkor) and recorded by a second camera that was coupled with a high-speed image intensifier (LaVision HS-IRO). An 80 mm × 80 mm GG 420 long-pass filter was placed in front of the fluorescence imaging setup. This filter has been used in engine experiments to not only suppress scattered laser light, but also to suppress a portion of the spark discharge signal, which can be damaging to the image intensifier [17]. The biacetyl fluorescence band extends largely between 420 and 550 nm. Thus, the filter does not significantly reduce PLIF signal levels. With these cameras, full frame resolution (600 × 800 pixels) can be achieved up to 4.8 kHz. The recording area was reduced to 416 × 416 pixels at 12 kHz, providing approximately a 20 × 20 mm^2 field of view (FOV). Each camera was equipped with 8 GB of onboard memory. Thus, approximately 32 500 consecutive frames could be recorded.

A target with a grid of one millimeter spatial frequency was placed at the jet center line to align the PIV and PLIF cameras. Once both cameras imaged the same FOV, the x–y location of each (Fig. 1) was adjusted with micrometer-controlled translation stages to ensure that specific points on the target were imaged onto the same pixel locations on the camera chips. Both cameras were aligned at a fixed location along the z-axis, the axial direction of the jet flow. This height was chosen to allow enough room to relocate the jet, so that images downstream of the jet exit could be recorded without the need to move the optical setup.

A pulse generator (Stanford Research Systems DG 535) was used to trigger the cameras and the laser at 12 kHz. There is an intrinsic delay (∼ 2 μs) between the clock trigger pulse to the camera and the beginning of the camera gate. The exposure time of each camera was set to 40 μs, which has been found useful during previous engine experiments to also capture the spark discharge when using a 355-nm interference filter [8]. To record the PLIF signal, the image intensifier was triggered by the PLIF camera during the 40-μs exposure time (Fig. 2). It was critical that the 100-ns laser pulse arrived during the intensifier gate time (1.35 μs) to successfully record this signal. Since the delay between the intensifier trigger pulse and the gate is negligible, the delay between the clock trigger and the laser pulses was adjusted while observing the strength of the PLIF signal. The optimum setting for this delay was 14 μs. The PIV camera trigger was synchronized with the PLIF trigger to ensure that the scattered and fluorescence signals were recorded simultaneously.

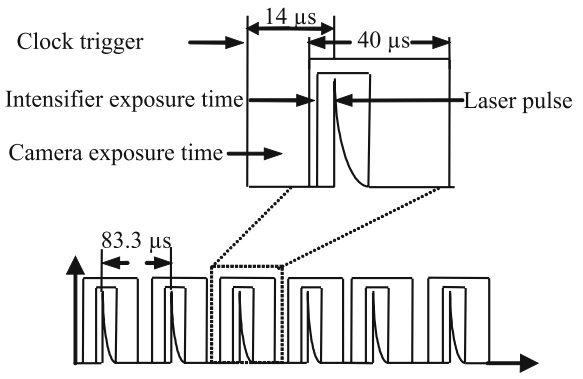

FIGURE 2 Timing diagram for the simultaneous velocity–scalar measurements in a jet using 355-nm excitation light. Note that the exposure times of the cameras overlap and only one is shown

The procedure for processing the PLIF images is relatively simple, particularly in comparison with processing requirements for PLIF images recorded in engine measurements. In the absence of in-cylinder engine features (i.e. spark plug, cylinder head, etc.), where laser light can scatter and also cause fluorescence from deposits, the background contribution to the images is low. To correct for spatial laser light intensity variations, the images were divided by an image taken under spatially homogeneous concentration conditions. Under such conditions, any variation in the PLIF signal is due only to variation in laser light intensity. This homogeneous condition was achieved using a quartz cuvette (28-ml volume) filled with a mixture of iso-octane and a drop of biacetyl (approximate biacetyl concentration ∼ 5×10^{-5} molar). One hundred images were averaged, and a 5 × 5 spatial filter was applied to obtain the calibration image. Once the jet images were corrected for laser light variation, a sliding 3 × 3 Gaussian filter was applied to reduce the influence of noise. Corrections for variations in laser pulse energy were not made, since they are only on the order of 3%. Isothermal and isobaric conditions in the jet eliminate the need for any corrections due to potential variations in absorption or fluorescence quantum yield. Biacetyl and air are fully premixed and thus phosphorescence emission is effectively

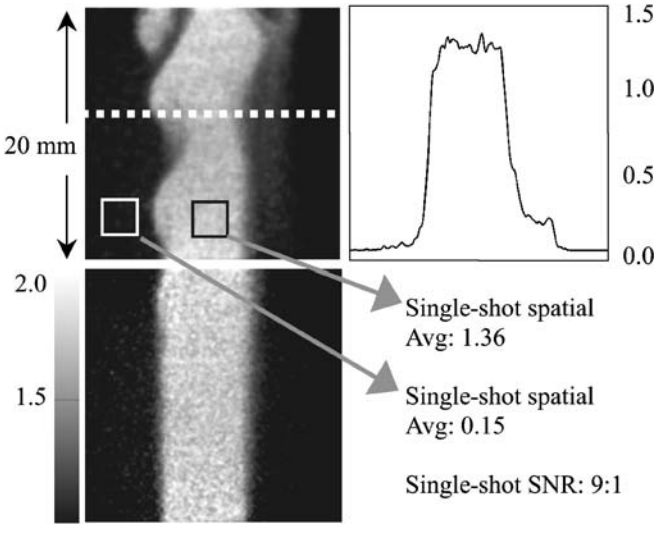

FIGURE 3 Biacetyl PLIF images from two separate experiments taken at different axial locations from the nozzle exit. The *top row* represents the condition on which this paper focuses. A profile is shown (extracted from the region approximated by the *dashed line*) to show relative signal levels across the jet

quenched anywhere in the jet. Overall, the light sheet-normalized images then represent a quantitative measurement of the relative concentration distribution of biacetyl in the jet. Examples of concentration fields at two different downstream locations are shown in Fig. 3. Steep spatial gradients are well resolved with an in-plane spatial resolution on the order of 59 μm. In addition to allowing full resolution of vortical structures in the jet, the signal-to-noise ratio is high enough to also allow the detection of faint flares of biacetyl that are occasionally visible on the right-hand side of the jet (see Fig. 3).

To obtain the vector fields, consecutive instantaneous images were cross correlated using a commercial software package (LaVision DaVis 7.1). A final interrogation window of 32 × 32 pixels with 50% overlap was used. As a result, the in-plane spatial resolution was 0.8 mm. A standard deviation operator was applied to replace spurious vectors with the mean of the four adjacent vectors, bringing the in-plane spatial resolution to 1.6 mm. No artificial vectors were introduced via interpolation.

The images include areas beyond the periphery of the jet, which are not seeded. A mask was applied to the raw images to exclude these areas from processing. Velocity vectors were computed inside the mask using a cross-correlation algorithm. As a final step during post processing, a 3 × 3 smoothing filter was applied to the vector fields to minimize error propagation when computing velocity gradients. The shear strain rate was calculated by taking first-order differences of the smoothed velocity field at each point.

3 Results and analysis

For demonstration of the simultaneous concentration and velocity imaging technique, data at a single axial location are discussed below. The jet Reynolds number was estimated based on velocity data extracted from PIV recordings 2 mm above the nozzle exit. Using the ensemble average velocity at this location (∼ 4 m/s), the pipe inner diameter (∼ 7 mm), and the kinematic viscosity of air (∼ 1.4×10^{-5} m^2/s), the Reynolds number (Re) is calculated to be 2000.

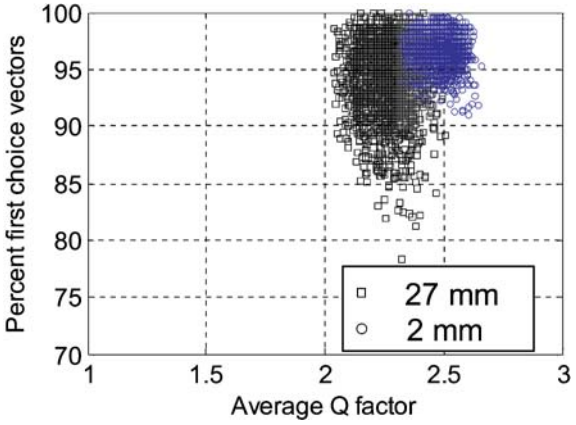

FIGURE 4 The average quality (Q) factor, which represents the ratio of the signal-to-noise peaks in the correlation map, demonstrates the high quality of the PIV measurements. A decrease in Q is noted for areas with rapid changes in spatial extent of the jet. This is due to the adaptive masking scheme that was employed, leading to small areas where no overlapping seeded areas are found

The fraction of vectors retained after post processing and the average quality (Q) factor, which represents the ratio of signal-to-noise peaks in the correlation map, are shown in the scatter plot of Fig. 4. The data correspond to 2000 vector fields calculated at two axial locations. The data for location 1, shown with circles, belong to the pipe exit positioned 2 mm below the FOV. The data for location 2, shown with squares, correspond to the pipe exit positioned 27 mm below the FOV. In 90% of the images, the retained vectors after post processing exceed 95% and 90% for locations 1 and 2, respectively. The discrepancy in percentage of vectors retained between the two locations can be attributed to the continuous roll-up and shedding of vortices at location 2. This phenomenon alters the effective (masked) area where vectors are computed between consecutive images and thus results in weaker correlations. The average Q factor lies above two in all cases, indicating that strong correlations were found. This compares well with the performance of more traditional PIV setups [14].

The left-hand column in Fig. 5 shows a sequence of velocity–scalar images that were recorded simultaneously 27 mm downstream of the nozzle. The time separation between successive images is 83.3 μs, matched to the requirements for best PIV evaluation. However, to visually highlight the changes in the flow, images are skipped in the display of Fig. 5. Therefore, note the time stamp on the images as well as the value indicating the frame number in the sequence of the original recording. In all images, the absolute velocity field has been superimposed onto the scalar field. The middle column of Fig. 5 shows the same sequence, but in this case the velocity has been displayed relative to a fixed seven-pixel displacement to reveal large-scale vortices arising from flow instabilities. The corresponding in-plane shear strain rate is shown in the right-hand column of Fig. 5. As expected, the largest strain values are localized along the jet shear layer, where the velocity gradients are largest.

Based on the liquid oil to gas volumetric ratio, physical processes such as adsorption and diffusion of biacetyl into the oil are not expected to contribute significantly to PLIF signal degradation. The interrogation volume, containing a well-mixed biacetyl–air blend and the PIV droplets, can be estimated as 2.56 mm^3 when using the interrogation window size of 32 × 32 pixels (1.6 mm × 1.6 mm) and the light-sheet thickness of 1.0 mm for the PIV measurement. This volume encloses 15 (approximately spherical) oil droplets of 1-μm diameter. The oil volume is then ∼ 8 μm^3, yielding an oil-to-biacetyl–air volume ratio of ∼ 3 ppb. This value suggests that the tracer interaction should be negligible. Influence of the PIV seeding on the biacetyl would be noticed as more intense points scattered about the field of view in the PLIF images. No qualitative difference in the PLIF images was observed with or without the presence of PIV oil droplets. The experimental data confirms that the interaction between the PIV and PLIF tracers is negligible.

To evaluate whether there was signal cross-talk, the biacetyl–air stream was temporarily blocked, allowing only the oil-seeded air to exit the pipe. In the absence of biacetyl, the 12-bit PLIF

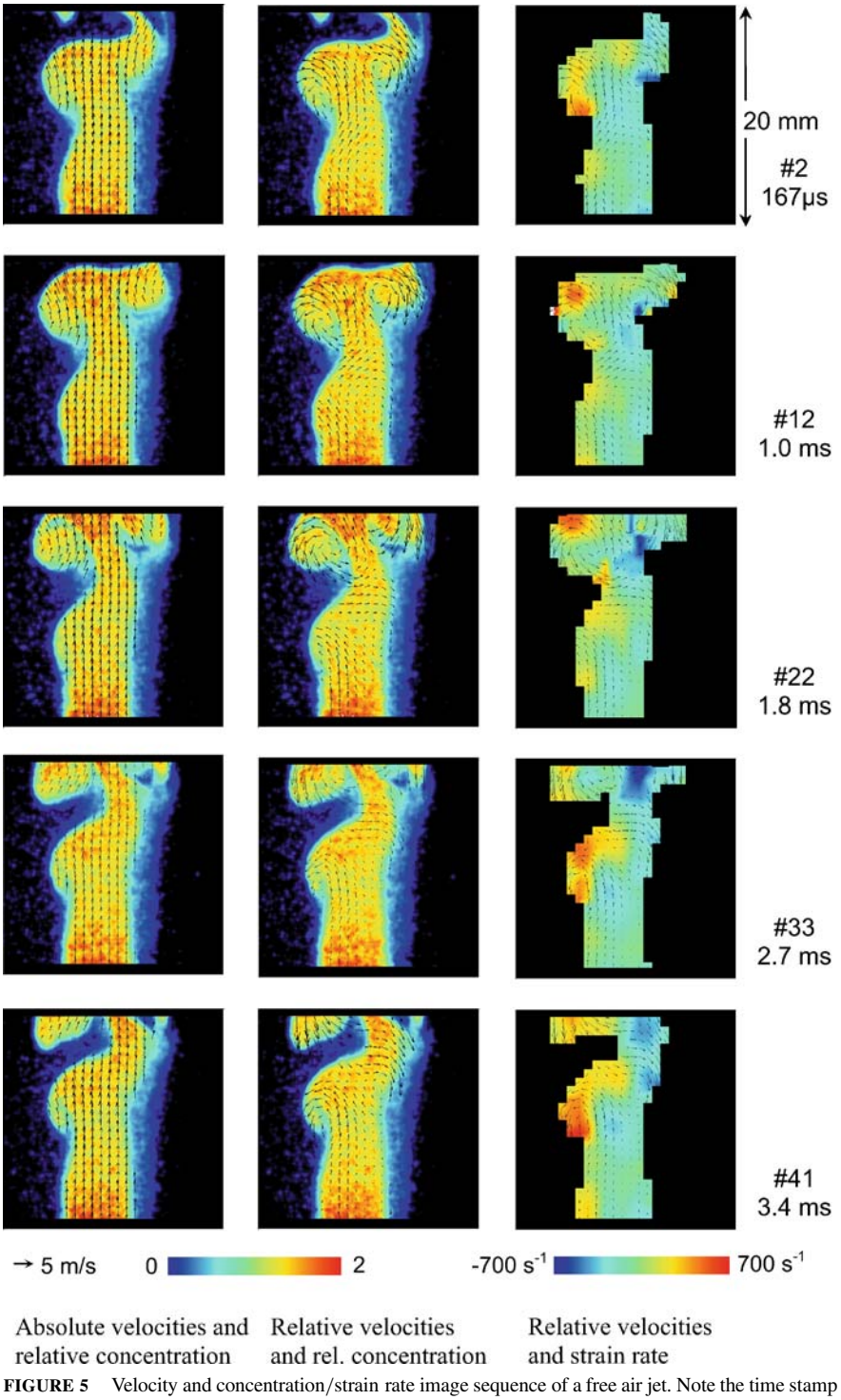

FIGURE 5 Velocity and concentration/strain rate image sequence of a free air jet. Note the time stamp and frame number on the right. Temporal and spatial resolution is adequate to resolve the evolution of the jet motion and structure

camera recorded a maximum signal of 175 counts, i.e. less than 15% of the maximum PLIF signal of 1200 counts. It is thought that the recorded signal results from a small fraction of 532-nm light being scattered by the oil droplets. Despite the HT 532-nm coating of the turning mirror M1 (Fig. 1) a small amount of the residual green light in the laser output is reflected and becomes part of the light sheet. A polarizing beam-splitting cube was placed in the laser beam path after M1. The separated beams clearly showed the presence of the 532-nm component. Future improvements of the setup therefore should include a Pellin–Broca prism to replace M1. While this can be effectively used to eliminate all of the unwanted 532-nm light in the light sheet, it is worth noting for the images presented here that the Mie scattering signal recorded by the PLIF camera is on the order of the noise level of PLIF measurements.

In any PLIF experiment, the ability to distinguish signal from noise is always a concern that needs some level of consideration. Single-shot SNR values are on the order of 9 : 1. This was determined from the ratio of the spatially averaged signal strength obtained in the core of the jet, where spatial variations are assumed to be low, to the average outside of the jet area (see Fig. 3). In contrast, biacetyl PLIF experiments conducted in the engine have generally been found to have lower SNR, on the order of 5 : 1 [7]. Reasons for the higher SNR here include fewer optics to absorb the signal light (i.e. the cylinder windows) and higher excitation energy available due to fewer optics in the excitation path. The biacetyl concentration used in this experiment is comparable to that used in engine experiments. However, signal strength at a higher temperature (i.e. in the engine) decreases significantly [17].

4 Conclusions

A high-speed technique that combines planar laser induced fluorescence detection of biacetyl and particle image velocimetry for simultaneous imaging of scalar and velocity fields was demonstrated at a frame rate of 12 kHz for up to 32 500 consecutive frames in an atmospheric pressure air jet. A single diode-pumped, frequency-tripled Nd-YAG laser was used in combination with two CMOS cameras. The UV sensitivity of a non-intensified CMOS camera was sufficient to use 355-nm Mie scattering for PIV measurements. Biacetyl fluorescence at wavelengths higher than 420 nm was recorded with a CMOS camera that was combined with a lens-coupled image intensifier. Interference between PIV and PLIF tracers was found to be negligible. Cross-talk between PIV and PLIF signals was low and mainly due to residual 532-nm light in the 355-nm beam. A strategy to completely eliminate it was devised and

discussed. The signal-to-noise ratio is about 9 for single-shot scalar images. The quality of the PIV results is equal to what is typically achieved with traditional high-power but low repetition rate PIV setups.

Since both the PLIF technique and PIV measurements have already been demonstrated separately in an optical engine [8, 17], it is anticipated, based on the findings presented here, that the simultaneous PIV-PLIF experiment can be successfully applied to the engine.

At the expense of added complexity and cost, the versatility of the technique can be enhanced with the use of two lasers. This will allow selecting the frame-to-frame time separation for PIV independent of the overall image rate. Thus, the trade-off between available pulse energy, frame size, and dynamic range of the PIV measurement is eliminated.

ACKNOWLEDGEMENTS This work was supported through the General Motors Collaborative Research Laboratory on Engine Systems Research at the University of Michigan. The authors are also grateful to J.F. Driscoll and S.L. Ceccio for the loan of the laser. C.M.F. acknowledges the receipt of an REA I fellowship from the Rackham Graduate School at the University of Michigan. J.D.S. is grateful to the Department of Undergraduate Education at the University of Michigan for a Graduate Student Instructorship.

REFERENCES

1 F. Zhao, M.-C. Lai, D.L. Harrington, Prog. Energ. Combust. Sci. **25**, 437 (1999)
2 J. Warnatz, U. Maas, R.W. Dibble, *Combustion*, 2nd edn. (Springer, Berlin, 1999)
3 C. Schulz, V. Sick, Prog. Energ. Combust. Sci. **31**, 75 (2005)
4 D.L. Reuss, Proc. SPIE **2005**, 413 (1993)
5 G. Josefsson, I. Magnusson, F. Hildenbrand, C. Schulz, V. Sick, Proc. Combust. Inst. **27**, 2085 (1998)
6 J. Hult, M. Richter, J. Nygren, M. Aldén, A. Hultqvist, M. Christensen, B. Johansson, Appl. Opt. **41**, 5002 (2002)
7 J.D. Smith, V. Sick, Appl. Phys. B **81**, 579 (2005)
8 C.M. Fajardo, V. Sick, Proc. Combust. Inst. **31** (2006), unpublished
9 C.D. Carter, J.M. Donbar, J.F. Driscoll, Appl. Phys. B **66**, 129 (1998)
10 J. Hult, G. Josefsson, M. Aldén, C.F. Kaminski, in: Proc. 10th Int. Symp. Applications of Laser Techniques to Fluid Mechanics, Paper 26.2, Lisbon, Portugal (2000)
11 P.S. Kothnur, M.S. Tsurikov, N.T. Clemens, J.M. Donbar, C.D. Carter, Proc. Combust. Inst. **29**, 1921 (2002)
12 C. Fukushima, L. Aanen, J. Westerweel, in: The Fifth JSME-KSME Fluids Engineering Conference, Session OS-5, Nagoya, Japan (2002), pp. 417–422
13 J.H. Frank, K.M. Lyons, M.B. Long, Combust. Flame **107**, 1 (1996)
14 M. Raffel, C.E. Willert, J. Kompenhans, *Particle Image Velocimetry: a Practical Guide*, 1st edn. (Springer, Berlin, 1998)
15 R. Adrian, Meas. Sci. Technol. **8**, 1393 (1997)
16 R.D. Keane, R. Adrian, Meas. Sci. Technol. **1**, 1202 (1990)
17 J.D. Smith, V. Sick, Proc. Combust. Inst. **31** (2006), unpublished